Available online at www.sciencedirect.com

ScienceDirect

Ceramics International 40 (2014) 1471–1479

CERAMICS INTERNATIONAL

www.elsevier.com/locate/ceramint

High-temperature corrosion of silicon carbide ceramics by coal ashes

M. Herrmann*, G. Standke, S. Höhn, G. Himpel, T. Gestrich

Fraunhofer Institute for Ceramic Technologies and Systems, IKTS, Dresden, Germany

Received 7 May 2013; received in revised form 5 July 2013; accepted 5 July 2013
Available online 11 July 2013

Abstract

New high-efficiency gasification reactors with higher temperatures and pressures and with different temperature cycles than previously require new types of refractory linings. Besides the oxide materials currently in use, SiC ceramics show great promise as refractories in the reducing atmospheres found in gasifiers. The behaviour of RSiC and SSiC materials was investigated in a flowing CO/H_2-containing Ar atmosphere with three different ashes (from basic to strongly acidic) in the temperature range between 1000 °C and 1300 °C. After dwell times of up to 100 h the cross sections of the materials were analysed by SEM and EDS. The results showed the high stability of the materials in all ashes. The porous RSiC materials showed small amounts of infiltration depending on the ash composition, but no destruction of the necks between the SiC grains was observed. Thermodynamic calculations simulating the conditions prevailing in a gasification reactor yielded similar phases to those obtained in the corrosive conditions used in the experiments. Due to the strongly reducing conditions the sulphates in the starting ashes reduced to sulphides of much lower corrosion activity

Keywords: C. Corrosion; Recrystallised silicon carbide; Silicon carbide

1. Introduction

Coal chemistry is gaining in importance due to the greater reserves of the fossil raw material coal and renewable biomass in comparison with those of natural oil and gas as starting materials for the petrochemical industry. The starting material in coal chemistry is a synthesis gas generated in gasification reactors. Higher gasifier efficiency can be achieved through a higher reaction temperature and a higher gas pressure. The reactor's service life is limited by the thermal shock resistance and the corrosion properties of the refractory lining [1–11]. Typical conditions for reactors are temperatures of around 1300 °C with a maximum temperature of 1600 °C and pressures of 25–40 bar as well as typical gas compositions of 55%–60% CO, 30%–35% H_2, 10%–15% CO_2 and 0.4%–1.5% H_2S [1,6,13]. The refractories of the reactor lining are subjected to a complex combination of stresses due to temperature, gas pressure, temperature fluctuations, abrasion by the solid fuel, the oxidising and reducing synthesis gas components and especially by chemical reactions with ash and slag of widely varying composition resulting from the variations in sources used [1,2,3–10]. Different corrosion mechanisms responsible for the failure of refractories have been observed [1,4–9]:

- Chemical dissolution of the refractory by molten slags resulting in a continuous but low wear rate. The reaction of the melt with the binder phase of the refractory can weaken the bonds inside the refractory until pullout of grains or parts of grains occurs. In the case of the widely used high chrome oxide refractories this rate of chemical attack can reach 3–5 mm/1000 h [1].
- Spalling [1] leading to a sudden loss of material (spalled surface layers can reach thicknesses of greater than 2 cm). This results from different damage mechanisms caused by slag infiltration and stresses caused by thermal shock or creep [1,6]. To avoid these processes a non-wetting surface and strong and chemically resistant bonds between the refractory grains are useful.
- Interaction with components of the gas phase (e.g. H_2S, H_2O or Cl-containing components).

*Corresponding author. Tel.: +49 35 125537700.
E-mail address: mathias.herrmann@ikts.fraunhofer.de (M. Herrmann).

0272-8842/$ - see front matter © 2013 Elsevier Ltd and Techna Group S.r.l. All rights reserved.
http://dx.doi.org/10.1016/j.ceramint.2013.07.031

– Thermal shock, insufficient creep resistance and abrasion can also limit the service life of the refractory.

The corrosion resistance of the refractory strongly depends on the ash composition which in turn strongly depends on the coal deposit or the biomass used. With respect to corrosive attack, a distinction can roughly be made between acidic, alkaline and (nearly) neutral ashes. Basic ashes are particularly harmful because they present a high corrosion risk even at relatively low temperatures due to the strong reduction of the viscosity of the slag and the high reactivity with oxide refractories. Acidic ashes with high SiO_2 contents strongly react with basic refractories such as MgO or spinel. However, the corrosive effects of the other ash components (e.g. sulphates and chlorine) must also be taken into consideration [9,12].

Numerous refractories for gasification reactors including high alumina, chromia alumina and silicon carbide materials have been evaluated [1–9,11,12]. Cr_2O_3-based and ZrO_2-based materials used in reactors have proven to be the most stable [1], but they also undergo corrosion which limits their lifetime [1–3,5,8]. SiC materials have also been investigated as refractories in gasification reactors [7,10]. However, the materials investigated were silicate-bonded or nitride-bonded materials in which corrosion mainly takes place in the binder phase. RSiC materials have not yet been tested, despite the fact that they have shown good stability as refractories in furnaces and refractory linings in waste incineration plants [11,14–18]. In contrast to silicate- or nitride-bonded materials in which the bond is formed by a secondary phase, recrystallised silicon carbide (RSiC) consists of SiC grains bonded directly to one another, allowing the high chemical stability of silicon carbide to be fully utilised. The result of this bonding is not only a fairly high strength, but also a relatively high thermal conductivity and hence a high thermal shock resistance. However, this material is produced at higher temperatures (up to 2400 °C) than is the case for clay- or nitride-bonded materials and is therefore slightly more expensive. Nevertheless, RSiC could be an interesting candidate for use in gasifiers due to its expected excellent corrosion resistance particularly under the reducing conditions prevailing in such applications and its high thermal shock resistance. The aim of this paper was to evaluate the stability of recrystallised SiC in coal ashes under reducing atmospheres. A solid state-sintered SiC was investigated for comparison purposes.

2. Experimental

Two commercial SiC materials were used for the investigations: a recrystallised silicon carbide with a porosity of 17% (mainly open porosity) and a dense sintered silicon carbide material with carbon and boron sintering additives. The properties of the materials are given in Table 1.

The corrosion experiments were carried out in a reactor tube furnace (Fig. 1) at temperatures of 1000 °C to 1300 °C with dwell times of 50 h and 100 h. The corrosive media were an acidic coal ash (S1), a basic coal ash (B1) and a mixed ash (BS) with a slightly acidic character. The chemical compositions and the phase compositions of the ashes are shown in Table 2. The different ashes were chosen because they were expected to exhibit strong differences in behaviour in acidic and basic ashes.

Table 1
Properties of the used SiC materials.

Material	Density (g/cm^3)	Open porosity (%)	Strength (MPa)	Strength after 8 thermo shocks from 950 °C to water (MPa)
RSiC	2.65	15	90 ± 8	14
SSiC	3.18	0.6	412 ± 46	Not measured

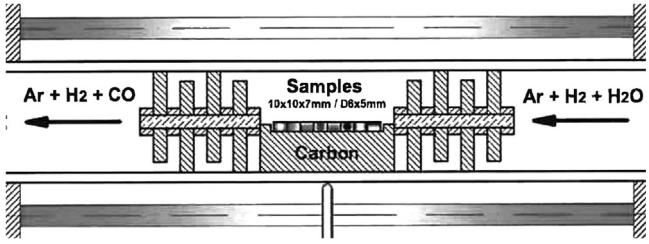

Fig. 1. Set up for the corrosion experiments.

A gas mixture consisting of 95% argon and 5% hydrogen with a dew point of 23 °C was guided over graphite moderators inside the reactor tube at a rate of 30 l/h. This was expected to result in the formation of a synthesis gas corresponding to the given reaction temperature according to the equilibrium reaction:

$$C+H_2O \Leftrightarrow CO+H_2$$

Thermodynamic calculations carried out in Factsage 6.3 [19] yielded a composition of the resulting gas atmosphere at 1300 °C of 7.4 vol% hydrogen, 2.5 vol% carbon monoxide and 91.1 vol% argon as the main components. The argon content was selected to limit the explosion potential of hydrogen and the poisoning potential of carbon monoxide based on the lengthy period of operation of the laboratory system and to ensure that sufficient carbon would be available for gas synthesis.

For the corrosion experiments cuboids with dimensions of $10 \times 10 \times 7$ mm^3 and brick-shaped material samples of the same geometry, but with a blind hole 6 mm in diameter × 5 mm in depth, were used for the RSiC materials. The SSiC samples were plates with dimensions of $8 \times 8 \times 7$ mm^3. For investigating the corrosion resistance of the materials, the cuboid samples were placed in graphite crucibles containing the various ashes, or ash was inserted into the brick openings. This allowed the effects of the sintered ash or the slag formed through melting of the ash, the temperature and the dwell time to be investigated on multiple materials under the same conditions in a single test.

Following high-temperature corrosion, the samples were investigated using light and electron microscopy. Cross sections were prepared through the SiC samples and the ashes/slag and the reaction layers formed during high-temperature corrosion were examined using an FESEM (field emission scanning electron microscope) and energy dispersive X-ray spectroscopy.

Table 2
Composition of the ashes [13].

Name	Composition		
Component	**S1** wt %	**BS (75% S1+25%B1)** wt %	**B1** wt %
C	1.8	4.6	12.8
Na_2O	1.3	5.1	16.7
K_2O	4.5	3.6	0.8
MgO	2.9	4.3	8.4
CaO	4.1	10.2	28.5
$Al2O_3$	25.5	19.4	1.3
SiO_2	49.6	38.2	3.9
$Fe2O_3$	7.2	7.9	10.0
TiO_2	1.2	1.0	0.2
SO_3	1.2	5.0	16.4
Type of the ash (basic/acid ratio)	**strong acidic 0.35**	**acidic 0.61**	**strong basic 12.1**
Mineral composition before corrosion	mostly amorphous (appr85%) SiO_2 $Al_6Si_2O_{13}$ Fe_2O_3; Fe_3O_4		$Ca_2Fe_2O_5$+Ca_2FeAlO_5 Na_2SO_4 $CaSO_4$ $CaCO_3$ CaO, MgO
Mineral composition after corrosion	Amorphous; Mullite, Quartz, α-Al_2O_3 $FeSi_x$ (?)	$CaAl_2Si_2O_8$, Na-Mg-K-Fe, Silikates,CaS, $MgSiO_3$ (?); $FeSi_x$(?)	CaS, Na-Ca-Mg-Fe-Alumosilikate, $CaO(CaOH_2)$, MgO(?), $FeSi_x$ (?)

Additionally, the ashes in the as-received state and after corrosion were analysed using X-ray diffraction (D8 diffractometer (Brucker), CuKα radiation, 40 kV, 30 mA, 2Θ range: 10°–90°). The behaviour of the ashes was also investigated using an STA 429 (Netzsch) in an Ar/H_2 atmosphere with a heating rate of 10 K/min.

Thermodynamic calculations using Factsage 6.3 [19] were carried out to elucidate the corrosion behaviour under the test conditions and to yield an understanding of the relationship between the reactions taking place under the test conditions and the reactions taking place under the conditions in a gasification reactor. The calculations were carried out using the sulphidic slag from the FACT database (Version 5.5.2012). This slag was chosen because the calculation without slags showed the decomposition of the sulphates into sulphides. The calculations were carried out with 50 times more gas than the mass of the ashes at a pressure of 25 atm for modelling the gasification reactor. For modelling the corrosive conditions the same ratio of ash to gas was used at a pressure of 1 atm.

3. Results and discussion

3.1. Thermodynamic calculations and thermoanalytical investigation of the ashes

The thermodynamic calculations of the interaction of SiC with the atmosphere of the gasifier revealed that SiC was not in thermodynamic equilibrium and decomposed into SiO_2 and C. However, this reaction is limited due to passivation of the surface by SiO_2 (as also observed in oxidising atmospheres). The high water vapour pressure in the gasifier can result in degradation of the passivation layer as in gas turbine environments [20], although the gas flow rates in the gasifier are much lower. The protective SiO_2 layer can be significantly altered by the ashes. Sulphates can strongly accelerate the oxidation and degradation of nonoxide ceramics [21,22]. The basic ash B1 contained a high amount of sulphates. However, the thermodynamic calculations showed that these sulphates decomposed into sulphides (Figs. 2 and 3).

The thermodynamic calculations of the condensed phases of the three ashes showed strong differences in the phases formed. For ash B1 the main phases CaS and CaO, MgO and a sulphide-containing liquid formed over the entire temperature range (Fig. 3).

In ashes S1 and BS the main phases were silicate-based phases. Iron sulphide was the only sulphide phase observed. The melt formation characteristics were also different (Fig. 3c). Ash BS was completely molten at temperatures higher than 1200 °C, whereas for B1 complete melting did not take place up to 1600 °C. The complete melting of ash S1 take place between those of the other two ashes.

Comparison of the phases formed under the conditions specified for the gasification reactor and under the conditions of the tube reactor experiments yielded very similar results, except in the case of ash B1 (Fig. 3) in which higher amounts of silicates and lower amounts of sulphides formed under the conditions of the corrosion experiments. This was caused by the different composition of the gas atmosphere (Fig. 2). The data revealed that Na_2O was the ash component with the highest vapour pressure, making it probable that the sodium would also evaporate during the corrosion experiments.

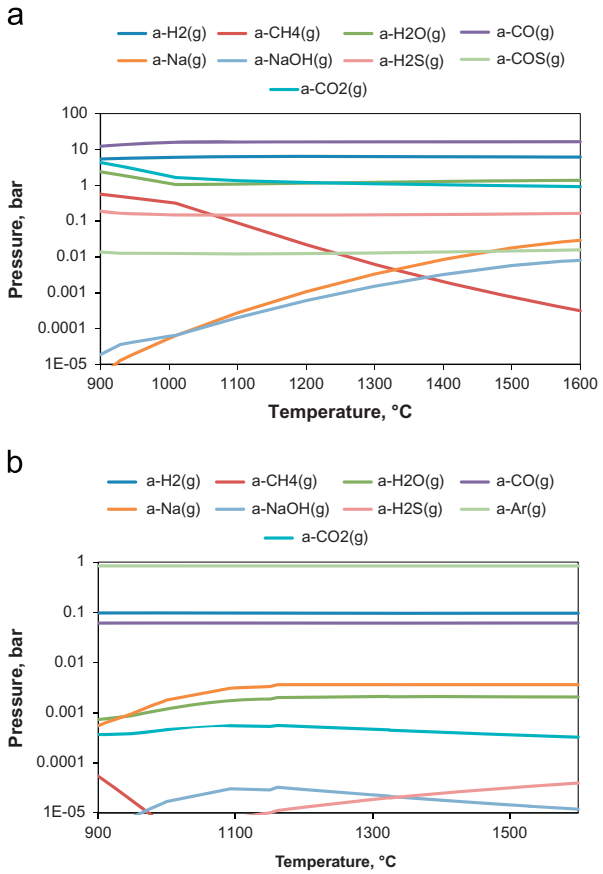

Fig. 2. Calculated composition of the gas phase as a function of the temperature in the gasification reactor and in the tube furnace for the corrosion experiments.

The amount of melt strongly depended on the Na_2O content in the ash. A reduction in the Na_2O content lowered the amount of liquid formed in the ashes (Fig. 3d).

The thermodynamic calculations demonstrated that the phase formation characteristics were similar in both the corrosive conditions and the simulated gasification reactor conditions. Therefore the corrosion experiments provided a first approximation of the corrosion stability of the SiC in the different ashes in a gasification reactor. However, differences in water vapour pressure under the different conditions could yield differences in corrosion behaviour.

The phases formed according to the thermodynamic calculations were confirmed by X-ray diffraction and DTA/TG analysis after the ashes were heated to 1300 °C (Figs. 4 and 5 and Table 2). The composition of the gas phase under both conditions and the resulting condensed phases for ash B1 are given in Figs. 2 and 3. Ash B1 showed the highest weight loss (37%) according to the DTA/TG results due to its high content of sulphates. The weight loss was caused not only by the decomposition of the sulphates, but also by the reduction of the oxide by the residual carbon. The strongest weight loss took place in ash B1 at 700°–800 °C and was accompanied by a strong endothermic peak at approximately 780 °C. This was most probably connected with the sulphate decomposition.

Consistent with the results of the thermodynamic calculations, no clear melting peaks were observed in the DTA traces of the three ashes. Ash S1 was amorphous and the amorphous phase only softened during heating. An indication of the softening was provided by the change in the slope of the base line at about 1000 °C, corresponding to the softening temperature of glasses with similar compositions.

The results of XRD analysis confirmed the different starting compositions of the three ashes. Ash S1 was mostly amorphous before and after corrosion, whereas in ash B1 the sulphates in the starting ash decomposed into sulphides (Table 2).

3.2. Results of the corrosion experiments

The stability of the SiC materials was tested at 1000°–1300 °C. After the corrosion experiments at 1000 °C the ashes were mostly solid and could easily be removed from the surfaces of the SiC materials on which they were situated. For ash B1 signs of local melting and gas formation were observed (see Fig. 6). This was an indication of decomposition of the sulphates. Sodium oxide was also detected in the ashes formed under these conditions by EDX. However, no significant interactions between the ashes and the SiC materials were observed.

In the corrosion experiments at 1300 °C the interactions with the ash were different for the three different ashes. The cross sections of the RSiC materials are given in Figs. 7–10. Ash B1 did not infiltrate into the material, but was found as sintered particles on the surface. In contrast, ashes S1 and BS infiltrated into the porous RSiC structure and filled the open pores. Ash BS exhibited the greatest extent of infiltration. This could be expected because this ash formed a liquid at the lowest temperature and had higher concentrations of Ca, Mg and Fe and hence a lower melt viscosity in comparison with ash S1. The infiltration of ash S1 occurred to a depth of 100–200 μm (Fig. 8b), whereas the slag completely infiltrated into the sample for ash BS (Fig. 10).

The EDX analysis of the melt revealed only a minor concentration of sodium oxide in the ashes after corrosion at 1300 °C, indicating that sodium evaporation occurred under the corrosive conditions. In addition to the silicate melt, a few Fe-rich inclusions (Figs. 7–9) were detected by EDX. These inclusions were also found to contain a small amount of silicon and were hence assumed to be silicides formed by reactions between the iron, iron oxides or sulphides and the SiC.

Fig. 11 shows the surface of the SSiC material after corrosion at 1000 °C in ash B1. Na_2O was also observed in the slag under these conditions. The cross sections of the SSiC materials corroded at 1300 °C for 50 h in the three ashes are given in Figs. 12–14. Detailed investigation of the interfaces between the slags and the SSiC material did not reveal any significant interactions. No infiltration along the grain boundaries of the dense SSiC material was found to take place (Figs. 12–14). This was consistent with the behaviour observed in the RSiC material which also showed no damage of the necks between the grains by the slag.

These results indicated the high stability of the SiC material under these conditions.

Cracks were observed in the infiltrated regions of the RSiC and in the slag layer on the surface of the SSiC, but almost

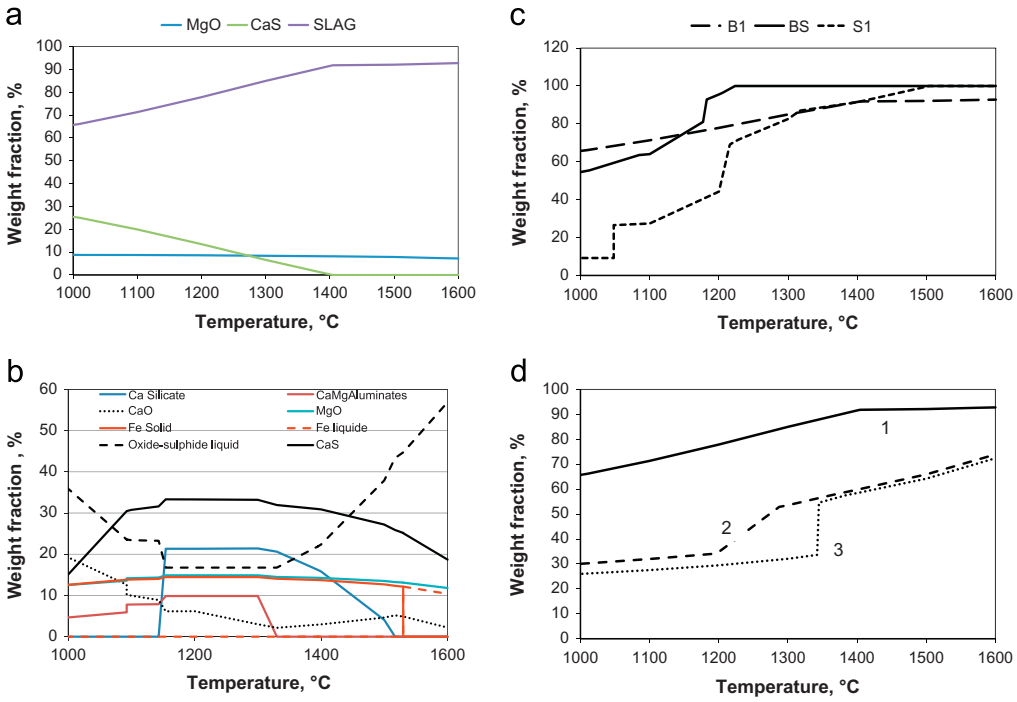

Fig. 3. (a): Calculated amount of the condensed phases of ash B1 as a function of the temperature in the gasification reactor and (b): in the tube furnace for the corrosion experiments, (c): Calculated weight fraction of the melt as a function of the temperature and (d): Calculated amount of liquid as a function of the Na_2O content in the slag (1- slag composition B1; 2- 10% of the Na_2O content of the standard composition B1, 3- 1% of the Na_2O content of the standard composition B1).

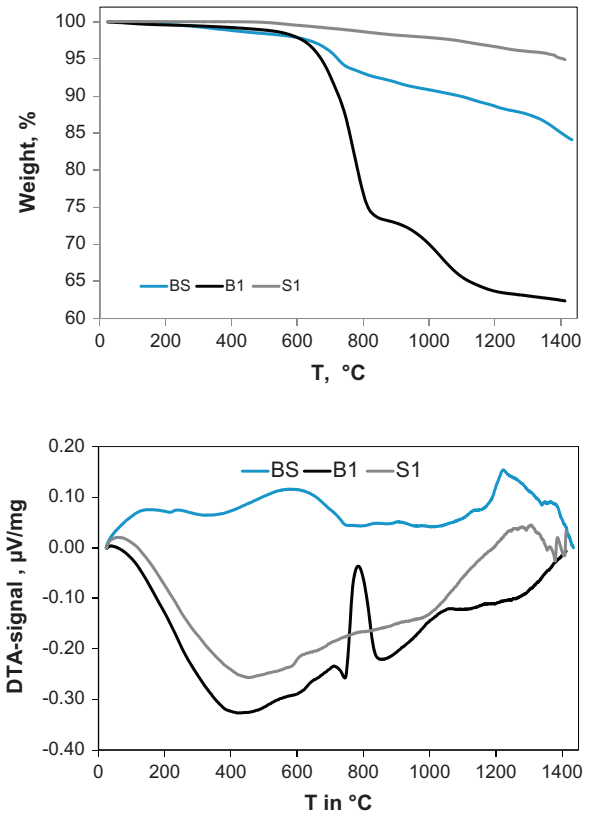

Fig. 4. TG and DTA signal of the three used ashes during heating in Ar 5%H2.

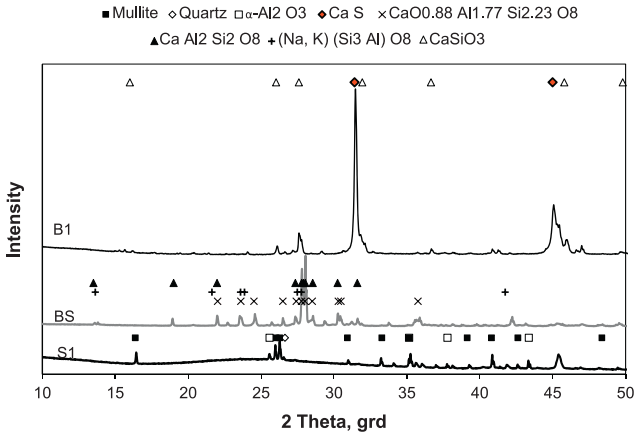

Fig. 5. X-ray diffraction data of the ashes after corrosion test at 1300 °C (100 h) (the main phases are marked).

exclusively in the infiltrated glassy phase and only very rarely in the dense SiC material. This could be attributed to the higher thermal expansion coefficient of the slag in comparison with that of the SiC, leading to tensile stresses in the glassy phase and compressive stresses in the SiC. This is different from the behaviour in Al_2O_3-/Cr_2O_3-based refractory materials. Therefore, spalling as a corrosion mechanism is less likely in these materials than in oxide refractories.

4. Conclusions

Recrystallised SiC and sintered silicon carbide (SSiC) were investigated in different coal ashes in a reducing carbon

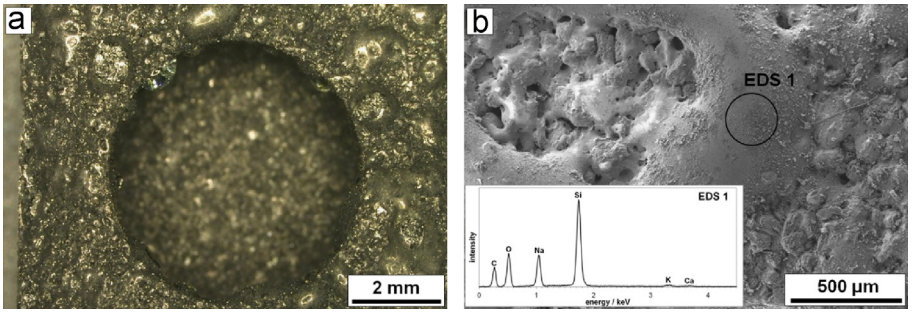

Fig. 6. Light microscopic image (a), SEM image (b) and EDS of RSiC material after corrosion at 1000 °C for 50 h in ash B1.

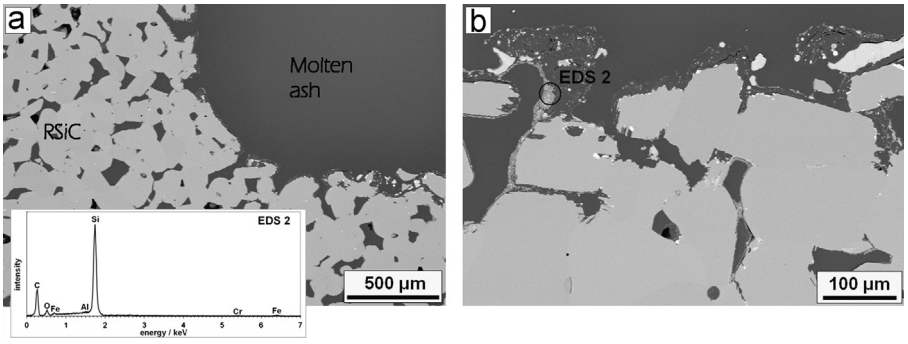

Fig. 7. SEM images (a, b) and EDS results of RSiC material after corrosion at 1300 °C for 50 h in ash B1.

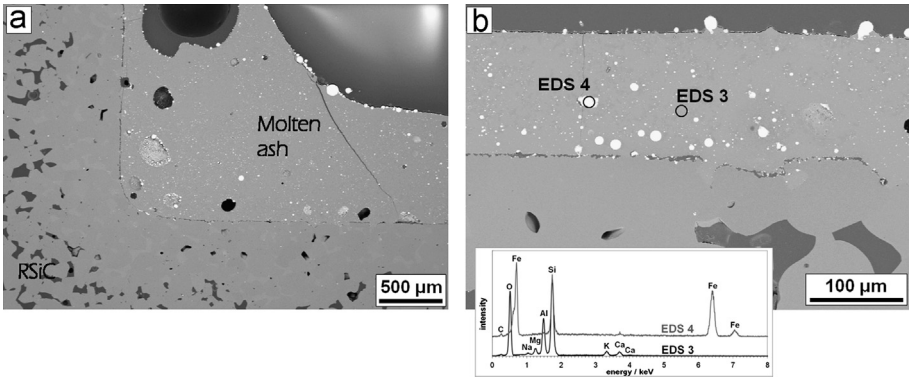

Fig. 8. SEM images (a, b) and EDS results of the RSiC material after corrosion at 1300 °C for 50 h in ash S1.

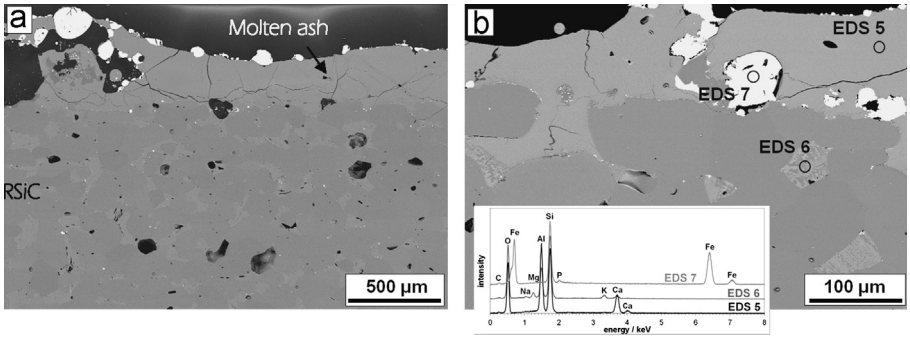

Fig. 9. SEM images (a, b) and EDS results of RSiC material after corrosion at 1300 °C for 100 h in ash BS.

monoxide- and hydrogen-containing atmosphere at temperatures between 1000 °C and 1300 °C. The materials were found to be extremely stable under these conditions in acidic and basic slags. Under the reducing conditions the sulphates in the starting ashes reduced to sulphides, but this had a minimal effect on the corrosion stability. This reduction of the sulphates

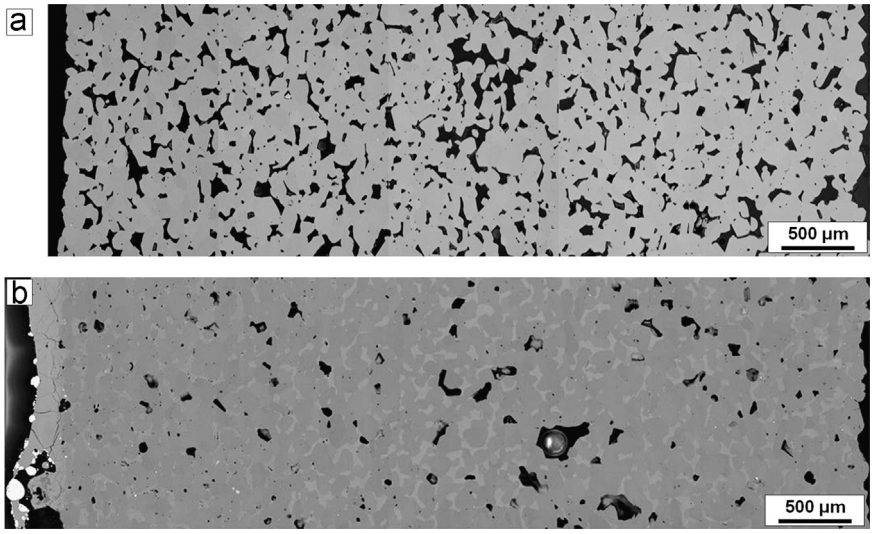

Fig. 10. SEM image (a) before and (b) after the complete infiltration of RSiC with BS-slag 1300 °C for 100 h.

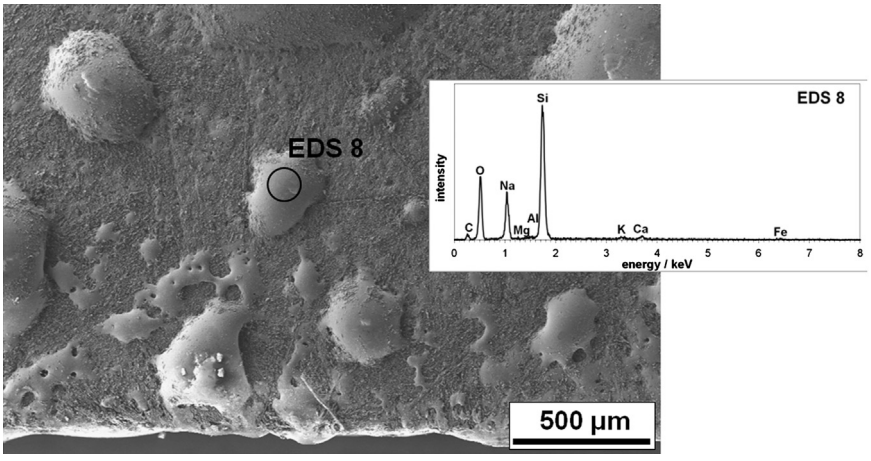

Fig. 11. SEM image and EDS results of SSiC material after corrosion at 1000 °C for 50 h in ash B1.

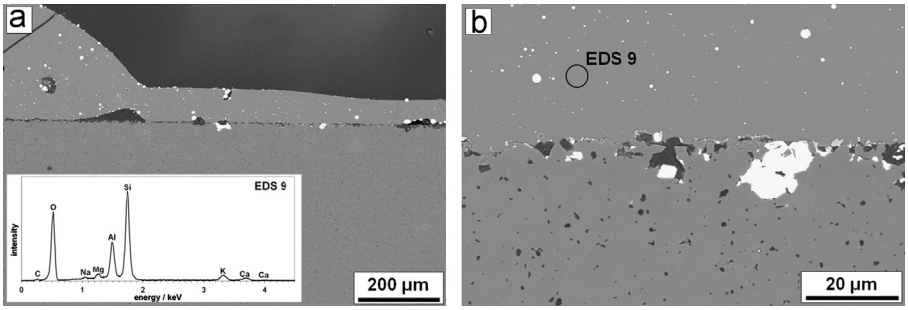

Fig. 12. SEM images (a, b) and EDS results of SSiC material after corrosion at 1300 °C for 50 h in ash B1.

resulted in a strong reduction in the corrosion activity of ash B1 because no sulphate melts were formed. When the ashes formed a silicate melt at the corrosion temperatures, infiltration into the open pores of the RSiC material was observed. The extent of infiltration was controlled by the viscosity, composition and amount of the formed melt. During cooling cracking occurred to a small extent in the formed glassy slag due to the higher thermal expansion coefficient of the glassy phase in comparison with that of the SiC. Crack formation was more pronounced in the alkaline earth-rich slags (BS) due to the higher thermal expansion mismatch. In contrast to oxide refractories, SiC has a thermal expansion coefficient equal to or less than that of the slag. Therefore, it can be expected that corrosion by spalling is less pronounced than would be the

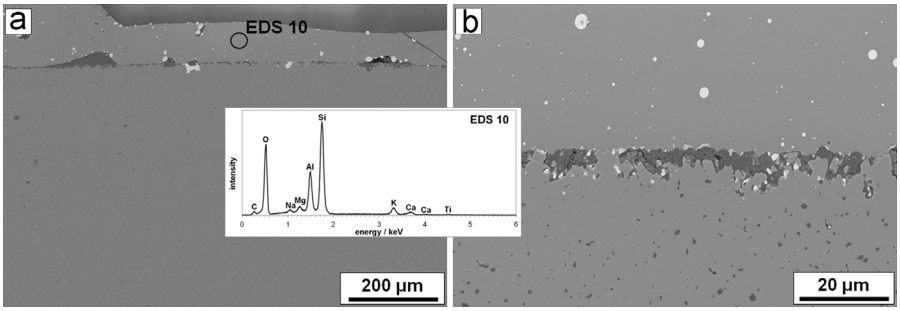

Fig. 13. SEM images (a, b) and EDS results of SSiC material after corrosion at 1300 °C for 50 h in ash S1.

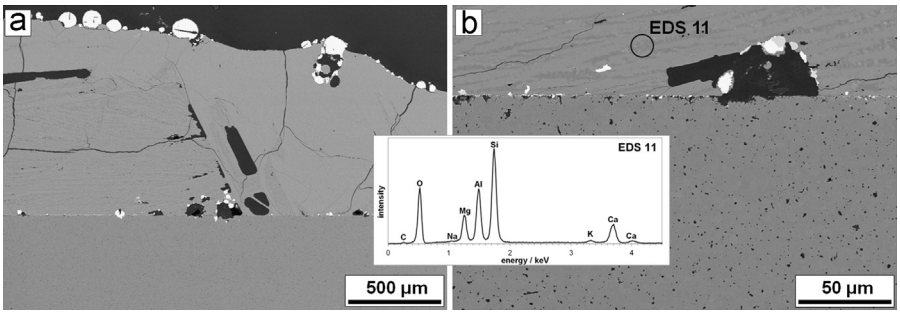

Fig. 14. SEM images (a, b) and EDS results of SSiC material after corrosion at 1300 °C for 100 h in ash BS.

case with oxide refractories. Investigation of the infiltrated area showed no substantial corrosion of the necks between the SiC grains, reflecting the much higher corrosion resistance of the RSiC in comparison with that previously observed for the nitride- and silicate-bonded SiC refractories [10]. No substantial attack of the dense SSiC materials was observed, indicating the high stability of the SSiC under these conditions as well. A further improvement in the stability of the RSiC refractories can be expected if the infiltration is further minimised. This can be obtained by reducing the wettability of the SiC by the melt, e.g. with carbon or formation of solid products by the reaction of the melt with a component such as ZrO_2 infiltrated into the pores of the RSiC.

According to the thermodynamic calculations the phases formed under the given corrosive conditions were similar to those formed in gasification reactors. The relatively simple experimental setup can therefore be used for initial selection of stable refractories for gasification reactors. However, a certain degree of uncertainty exists due to the fact that the water vapour pressure is higher in a gasification reactor than in the corrosion experiments.

Acknowledgements

This research was conducted under the auspices of the German Energy Raw Material Centre within the framework of the project ‘Technologies for the post-oil era'. The German Energy Raw Material Centre is promoted mainly by the German Federal Ministry of Education and Research (BMBF) as well as the companies Vattenfall Europe Mining & Generation, RWE Power, ROMONTA and MIBRAG, all acting as direct network partners funding the research project. This alliance is strengthened by a further 14 partners providing complementary project support.

References

[1] L. San-Miguel, ChrHisM Schumann, High performance refractories for gasification reactors refractories, WORLDFORUM 3 (2011) 4–7.
[2] K. Kwong, A. Petty, J.P. Bennett, R. Krabbe, H. Thomas, Wear mechanisms of chromia refractories in slagging gasifiers, International Journal of Applied Ceramic Technology 6 (2007) 503–513.
[3] M.S. Crowley, Refractory problems in coal gasification reactors, American Ceramic Society Bulletin 54 (1975) 1072–1074.
[4] C.P. Dogan, J.P. Bennett, K-S Kwong, R.E. Chinn, Refractory loss in slagging gasifiers, in: Proceedings of the Unified International Technical Conference on Refractories, 1 (2001) 270–275.
[5] C.R. Kennedy, R.B. Poeppel, Corrosion resistance of refractories exposed to molten acidic coal-ash slags, Interceram 3 (1978) 221–226.
[6] P. Gehre, C.G. Aneziris, Investigation of slag containing refractory materials for gasification processes, Journal of the European Ceramic Society 32 (2012) 4041–4042.
[7] R.E. Dial, Refractories for coal gasification and liquefaction, American Ceramic Society Bulletin 54 (1975) 640–643.
[8] W.T. Bakker, S. Greenberg, M. Trondt, U. Gerhardus, Refractory practice in slagging gasifiers, American Ceramic Society Bulletin (1984) 870–87663 (1984) 870–876.
[9] J.A. Bonar, C.R. Kennedy, R.B. Swaroop, Coal-ash slag attack and corrosion of refractories, American Ceramic Society Bulletin 59 (1980) 473–478.
[10] J. Poirier, L. Colombel, P. Prigent, The corrosion mechanisms of SiC refractory lining in waste incineration plants and in reactors of biomass gasification, in Proceedings of the International Coliquim Reference, 2009, pp. 49–52.
[11] G Routschka, Feuerfeste Werkstoffe, 5 Auflage, Vulkan (2011) 60–64.
[12] M. Müller, K. Hilpert, L. Singheiser, Corrosion behavior of chromium-free ceramics for liquid slag removal in pressurized pulverized coal combustion, Journal of the European Ceramic Society 29 (2009) 2721–2726.

[13] H. Gutte, M. Klinger, TU-BAF, 2012, private communication.
[14] V. Köhne, H. Knorth, H.D. Pötsch, Zur Haltbarkeit feuerfester Werkstoffe in kommunalen Müllverbrennungsanlagen, VGB Kraftwerkstechnik 68 (1988) 1279–1286.
[15] W. Völker, Bewährte und neue SiC-Feuerfest-Baustoffe für Müllverbrennungsanlagen, in: Proceedings of the 40th International Colloquium on Refractories, Aachen, 1987, pp. 174–175.
[16] St Mulch, I. Elstner, D. Grimm, H. Kinne, Korrosionsvorgänge an feuerfesten Werkstoffen in kommunalen Müllverbrennungsanlagen, VGB Kraftwerkstechnik 78 (1998) 70–74.
[17] W. Völker, Bewährte und neue SiC-Feuerfest-Baustoffe für Müllverbrennungsanlagen, in: Proceedings of the 40th International Colloquium on Refractories, Aachen, 1987, pp. 174–175.
[18] St Mulch, I. Elstner, D. Grimm, H. Kinne, Korrosionsvorgänge an feuerfesten Werkstoffen in kommunalen Müllverbrennungsanlagen, VGB Kraftwerkstechnik 78 (1998) 70–74.
[19] Factsage 6.3, Thermfact and GTT-Technology, FactPS database, 2012.
[20] M. Fritsch, H. Klemm, M. Herrmann, A. Michaelis, B. Schenk, The water vapour hot gas corrosion of ceramic materials, Ceramic forum international: CFI, Berichte der Deutschen Keramischen Gesellschaft, vol. 87 (11–12) 2007.
[21] N. Jacobson, D.S. Fox, Molten-Salt Corrosion of Silicon Nitride: II, Sodium Sulfate, Journa of American Ceramic Society, 71, 139–148.
[22] K.G. Nickel, P. Quirmbach, J. Pötschke, High temperature corrosion of ceramics and refractory materials, Shreir's Corrosion 1 (2010) 668–690.